Global properties of Stochastic Loewner evolution driven by Lévy processes

P. Oikonomou, I. Rushkin, I. A. Gruzberg, L. P. Kadanoff

The James Franck Institute, The University of Chicago
5640 S. Ellis Avenue, Chicago, Il 60637 USA

January 14, 2008

Abstract

Standard Schramm-Loewner evolution (SLE) is driven by a continuous Brownian motion which then produces a trace, a continuous fractal curve connecting the singular points of the motion. If jumps are added to the driving function, the trace branches. In a recent publication [1] we introduced a generalized SLE driven by a superposition of a Brownian motion and a fractal set of jumps (technically a stable Lévy process). We then discussed the small-scale properties of the resulting Lévy-SLE growth process. Here we discuss the same model, but focus on the global scaling behavior which ensues as time goes to infinity. This limiting behavior is independent of the Brownian forcing and depends upon only a single parameter, α, which defines the shape of the stable Lévy distribution. We learn about this behavior by studying a Fokker-Planck equation which gives the probability distribution for endpoints of the trace as a function of time. As in the short-time case previously studied, we observe that the properties of this growth process change qualitatively and singularly at $\alpha = 1$. We show both analytically and numerically that the growth continues indefinitely in the vertical direction for $\alpha > 1$, goes as $\log t$ for $\alpha = 1$, and saturates for $\alpha < 1$. The probability density has two different scales corresponding to directions along and perpendicular to the boundary. In the former case, the characteristic scale is $X(t) \sim t^{1/\alpha}$. In the latter case the scale is $Y(t) \sim A + Bt^{1-1/\alpha}$ for $\alpha \neq 1$, and $Y(t) \sim \ln t$ for $\alpha = 1$. Scaling functions for the probability density are given for various limiting cases.

1

Contents

1 Introduction

The study of random conformally-invariant clusters that appear at critical points in two-dimensional statistical mechanics models has been made rigorous with the invention of the so-called Schramm-Loewner evolution (SLE) [2]. SLE refers to a continuous family of evolving conformal maps that specify the shape of a part of a critical cluster boundary. By now SLE has been justly recognized as a major breakthrough, and there are several review papers and one monograph devoted to this beautiful subject, see Refs. [3, 4, 5, 6, 7, 8, 9, 10]

SLE describes a curve, called trace, growing with time from a boundary in a two-dimensional domain which is usually chosen to be the upper half plane. SLE is based on the Loewner equation in which the shape of the growing curve is determined by a function of time $\xi(t)$ which in SLE is taken to be a scaled Brownian motion. Such a choice of the driving function produces continuous stochastic, fractal and conformally invariant curves, — the kind that appears as the scaling limit of various interfaces in many two-dimensional critical lattice models and growth processes of statistical physics. Well-known examples include boundaries of the Fortuin-Kastelyn clusters in the critical q-state Potts model, loops in the $O(n)$ model, self-avoiding and loop-erased random walks.

In Ref. [1] we generalized SLE to a broader class for which $\xi(t)$ is a Markov process with discontinuities. More specifically, we have studied the Loewner evolution driven by a linear combination of a scaled Brownian motion and a symmetric stable Lévy process. The growing curve then exhibits branching. This generalized process might be useful to describe many tree-like growth processes, such as branching polymers and various branching growth processes which evolve in time.

Such generalized SLEs driven by Lévy processes (Lévy-SLE for short) have also been of interest to mathematics community. Our results [1] on various phase transitions in Lévy-SLE have been put on rigorous basis in Ref. [11], and further properties have been studied in Refs. [12, 13]. The interest of mathematicians in these Lévy-SLE processes is partially motivated by the suggestion [13, 14] that they may produce fractal objects with large values of multifractal exponents for harmonic measure. Harmonic measure can be thought of as the charge distribution on the boundary of a conducting cluster. On fractal boundaries such a distribution is a multifractal, and in the case of critical clusters (whose boundaries are SLE curves) the full spectrum of multifractal exponents has been obtained analytically, see Refs. [14, 15, 16, 17, 18] for various derivations and discussion.

While our previous paper [1] focused on local properties of Lévy-SLE, here we study the global behavior of the growth in the upper half plain. The present paper is structured as follows. In Section 2 we define our model and briefly state our previous results on phase transitions in the local behavior of the model. We also present our new results on the global behavior of Lévy-SLE. In Section 3 we derive the Fokker-Planck equation governing the evolution of the probability distribution for the tip of the Lévy-SLE. The equation is our main tool for analysis of the long time global behavior of the growth. We give a qualitative description of the growth and explain the approximations that go into the solution of the Fokker-Planck equation in Section 4. Actual solution of the Fokker-Planck equation and comparison with results from numerically calculated trajectories is given in Section 5. We conclude in Section 6. Some technical details are presented in Appendices.

2   The model and the results, old and new

Loewner evolution is a family of conformal maps that appears as the solution of the Loewner differential equation (see, for example, Ref. [3] for details)

$$\partial_t g_t(z) = \frac{2}{g_t(z) - \xi(t)}, \qquad\qquad g_0(z) = z. \qquad (1)$$

valid at any point z in the upper half plane until (and if) this point becomes singular at some (possibly infinite) time τ_z: $\xi(\tau_z) = g_{\tau_z}(z)$. The set of all singularities is called the hull and the point at which the hull grows is called the tip. The tip $\gamma(t)$ is defined via its image $\xi(t) = g_t(\gamma(t))$. More formally,

$$\gamma(t) = \lim_{w \to \xi(t)} g_t^{-1}(w), \qquad (2)$$

where the limit is taken in the upper half plane. The trace is the path left behind by the tip (the existence of the trace in the setting of this paper has been shown in Ref. [12]). The shape of the growing trace (and the hull) is completely determined by the driving function $\xi(t)$. At any time the function $g_t(z)$ conformally maps the exterior of the growing hull to the upper half plane, see Fig. 1. We refer to the z plane where the growth occurs as "the physical plane", and to the w plane as "the mathematical plane".

Naturally, if $\xi(t)$ is a stochastic process the shape of the growing trace is also stochastic. The growth process is then a stochastic (Schramm-) Loewner

4
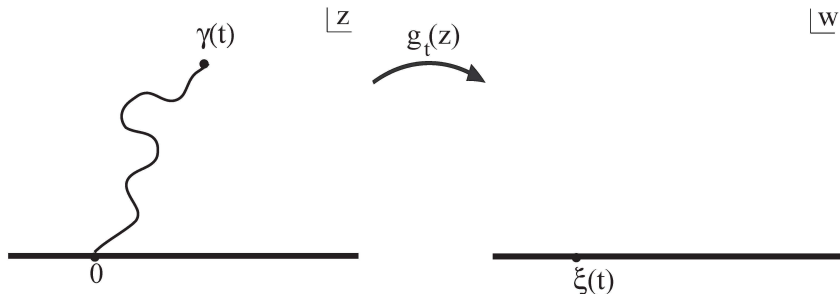
Figure 1: The Loewner evolution shown for the case when the growing hull is a smooth curve. The complement of the segment of the curve (up to its tip $\gamma(t)$) in the "physical" z plane is mapped to the entire upper half of the "mathematical" w plane by the function $g_t(z)$.

evolution (SLE). The standard SLE has a driving function $\xi(t) = \sqrt{\kappa}B(t)$, where $B(t)$ is a normalized Brownian motion and $\kappa > 0$ is the diffusion constant. Many important properties of this process have been established in Ref. [19].

In Ref. [1] we have generalized SLE to

$$\xi(t) = \sqrt{\kappa}B(t) + c^{1/\alpha}L_\alpha(t), \tag{3}$$

where $L_\alpha(t)$ is a normalized symmetric α-stable Lévy process [20, 21, 22, 23], and $c > 0$ is the "diffusion constant" associated with it. The process $L_\alpha(t)$ is composed of a succession of jumps of all sizes. Unlike a Brownian motion, $L_\alpha(t)$ is discontinuous on all time-scales. Therefore, the addition of a Lévy processes to the driving force of SLE introduces branching to the trace.

The probability distribution function of $c^{1/\alpha}L_\alpha(t)$ is given by the Fourier transform

$$P(x,t) = \int_{-\infty}^{\infty} \frac{dk}{2\pi} e^{-ikx} e^{-ct|k|^\alpha}. \tag{4}$$

As it is known in the theory of stable distributions [23], only for $0 < \alpha \leqslant 2$ this Fourier transform gives a non-negative probability density. For $0 < \alpha < 2$ the function $P(x,t)$ decays at large distances as a power law:

$$x \to \infty : \quad P(x,t) \sim \frac{ct}{|x|^{1+\alpha}}, \tag{5}$$

5

so that the process scales as

$$\langle |L_\alpha(t)|^\delta \rangle \propto t^{\delta/\alpha} \qquad (6)$$

for any $\delta < \alpha$. For $\delta \geqslant \alpha$ this average is infinite. For $\alpha = 2$ the process $L_2(t)$ is the standard Brownian motion $B(t)$ and $P(x,t)$ is Gaussian.

We studied the short-distance properties of the Lévy-SLE process in Ref. [1]. At short times and distances the process is dominated by the Brownian motion and the deterministic drift term (see Eq. (13)), whereas at long times it is dominated by Lévy flights. The crossover between short and long time behavior happens at the time

$$t_0 \sim \left(\frac{1}{c^2} \right)^{1/(2-\alpha)}. \qquad (7)$$

This also defines a spatial crossover at length scales $l_0 \propto \sqrt{t_0}$. For scales smaller than l_0 the trace behaves like standard SLE, while for scales much larger than l_0 it spreads in the x direction forming tree-like structures.

In our previous paper [1], using both analytic and numerical considerations, we determined the probability that a point on the x axis is swallowed by the trace. The trace shows a qualitative change in its small-distance, small-time behavior as κ and α each pass though critical values, respectively at four and one. The transition at $\kappa = 4$ is quite analogous to the known transition of standard SLE [19]. For the new transition at $\alpha = 1$, the trace forms isolated trees when $\alpha < 1$ or a dense forest when $\alpha > 1$.

The latter phase transition at $\alpha = 1$ was recently studied rigorously in Ref. [11] which expanded the implications of the phase transition to the whole plane at the limit $t \to \infty$. For $\kappa > 4$ a point in the upper half plane is swallowed almost surely for $\alpha > 1$, while it is swallowed with probability smaller than one for $\alpha < 1$. For $\kappa < 4$ and $0 < \alpha < 2$ the swallowed points on the plane form a set of measure zero.

The large-scale implications of the $\alpha = 1$ transition can be seen in Figure 2 which shows the shape of the trace at long times. For $\alpha < 1$ the stochastic evolution produces isolated tree-like structures which are limited in height. For $\alpha > 1$ the evolution produces an "underbrush" in which structures pile on one another and thereby continue to increase their height.

In the rest of the paper we establish the following. The growth at long times is characterized by two very different length scales $X(t)$ and $Y(t)$ (with $X(t) \gg Y(t)$) which can be thought of as the typical size of the growing hull
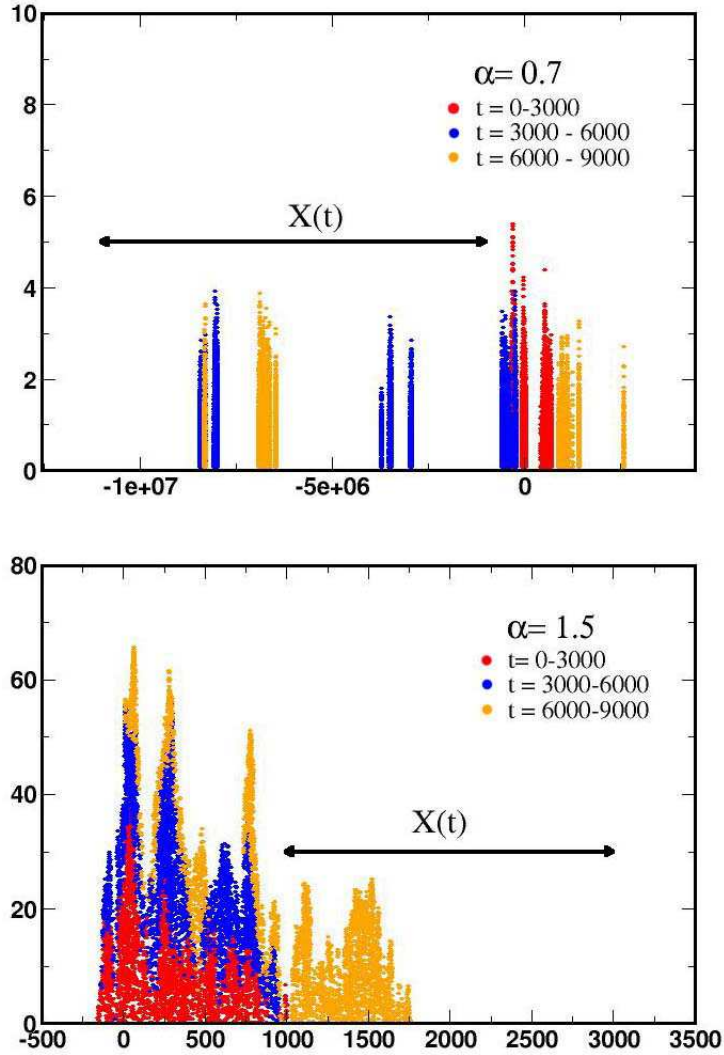
Figure 2: Examples of traces produced by Lévy-SLE at long times, up to $t = 9000$. For the first, second and last thirds of the time interval, the traces are correspondingly colored red, blue, and yellow. Top panel: $\alpha = 0.7$. The trace looks like many isolated trees whose height saturates at long times. Bottom panel: $\alpha = 1.5$. Now the tip of the growing trace keeps landing on the previously grown "bushes" so that the trace extends indefinitely in the vertical direction as time increases. Notice the difference in scales for the y axis between the two panels, as well as the much larger spread in the x direction in the top panel. The trace was produced using stable Lévy forcing and $c = 10$, time step $\tau = 10^{-3}$. The trace was calculated only at times when the forcing makes a large jump $d\xi > \sqrt{200\tau}$.

7

in the x and y directions. More specifically, we find that

$$X(t) \sim t^{1/\alpha}, \quad 0 < \alpha < 2, \tag{8}$$

$$Y(t) \sim \begin{cases} A + Bt^{1-1/\alpha}, & \alpha \neq 1, \\ \ln t, & \alpha = 1. \end{cases} \tag{9}$$

(The constants A and B depend upon α.) These scales enter the scaling form of the joint probability distribution $\rho(x, y, t)$ for the real and imaginary parts of the tip $\gamma(t)$ of the Lévy-SLE, for which we give explicit results in various limiting cases in Section 5, where we also compare analytical results with extensive numerical simulations.

3   Derivation of the Fokker-Planck equation

We are interested in characterizing the probability distribution for the point $\gamma(t)$ at the tip of the trace in the ensemble provided by different realizations of the SLE stochastic process. Eq. (2) implies then that we should study the inverse map g_t^{-1}. However, this is rather difficult, since the map g_t^{-1} satisfies a partial differential equation instead of an ODE. There is a way out which is rather well known and has been successfully used before [13, 14, 19]. It happens that one needs to consider the backward time evolution:

$$\partial_t f_t(w) = -\frac{2}{f_t(w) - \xi(t)}, \qquad\qquad f_0(w) = w. \tag{10}$$

The relation of the original Loewner evolution (1) and the backward one (10) in the stochastic setting is as follows. If $\xi(t)$ is a symmetric (in time) process with independent identically distributed increments, which is the case for a Lévy process, then it is easy to show that for any fixed time t the solution $f_t(w)$ of the backward equation (10) has the same distribution as $g_t^{-1}(w - \xi(t)) + \xi(t)$, see Refs. [13, 19]. Using the symbol $\overset{d}{=}$ for equality of distributions for random variables, we can write

$$f_t(w) \overset{d}{=} g_t^{-1}(w - \xi(t)) + \xi(t). \tag{11}$$

It is useful to introduce a shifted conformal map

$$h_t(z) = g_t(z) - \xi(t), \tag{12}$$

for which the Loewner equation acquires the Langevin-like form:

$$\partial_t h_t(z) = \frac{2}{h_t(z)} - \partial_t \xi(t), \qquad\qquad h_0(z) = z, \tag{13}$$

8

assuming that ξ vanishes at $t = 0$. The first term is a deterministic drift and the second — a random noise. The tip $\gamma(t)$ is now mapped to zero, and this can be taken as the definition of the tip. More formally,

$$\gamma(t) = \lim_{w \to 0} h_t^{-1}(w) \tag{14}$$

where the limit is taken in the upper half plane.

In terms of the shifted map the equality of distributions (11) can be written as

$$f_t(w) - \xi(t) \overset{d}{=} h_t^{-1}(w). \tag{15}$$

The left hand side $z_t \equiv f_t(w) - \xi(t)$ of this equation satisfies the Langevin-like equation

$$\partial_t z_t = -\frac{2}{z_t} - \partial_t \xi(t), \qquad\qquad z_0 = w, \tag{16}$$

and in particular, if we set $w = 0$ in this equation, the resulting stochastic dynamics should be the same as that of the tip of the trace $\gamma(t)$.

Before we convert the Langevin-like equation (16) to our main analytical tool, the corresponding Fokker-Planck equation, let us review again the correspondence between the forward and backward flows and illustrate it with figures. Equation (13) describes a flow in which $w_t = h_t(z)$ follows a trajectory of a particle in the w plane, z being its initial position. Separating the real and imaginary parts of $w_t = u_t + iv_t$, we get a system of coupled equations

$$\partial_t u_t = \frac{2u_t}{u_t^2 + v_t^2} - \partial_t \xi(t), \qquad\qquad u_0 = x,$$
$$\partial_t v_t = -\frac{2v_t}{u_t^2 + v_t^2}, \qquad\qquad v_0 = y, \tag{17}$$

describing such a trajectory. As in many modern versions of dynamics, all initial conditions and hence all trajectories are considered at the same time, forming an ensemble. Two such trajectories are presented on the top panel in Fig. 3. For a generic initial point z the trajectory w_t goes to infinity in the horizontal u direction, while the vertical coordinate v_t monotonously decreases. However, if the initial point happens to be a point $\gamma(T)$ on the SLE trace, the forward trajectory hits the origin in the mathematical plane exactly at time T.

Conversely, we can fix a point w in the mathematical plane and follow the motion of its image z_t under the map $f_t(w) - \xi(t)$ in the physical plane, with
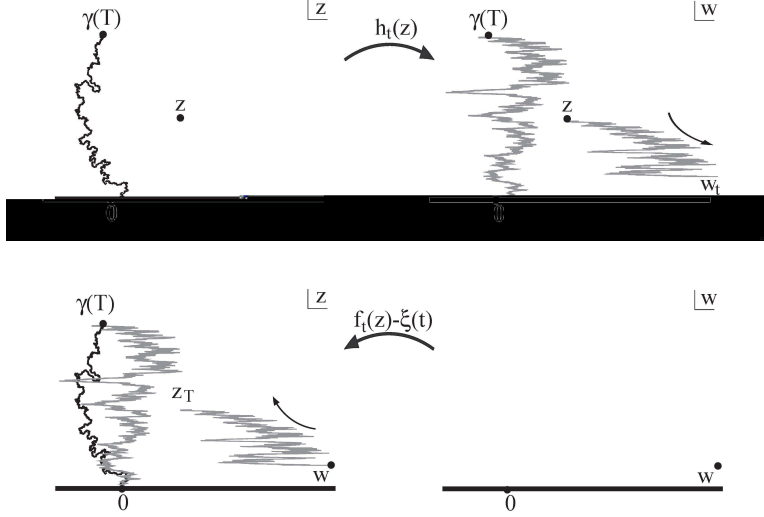
Figure 3: Top panel: two trajectories in the forward flow. Bottom panel: the corresponding trajectories in the backward flow. Curved arrows indicate the flow of time. In both cases the flow trajectories are shown in grey, while the black line represents an SLE trace. The trajectories on the bottom panel have been produced with the same noise realization as used for the forward evolution, reversed in time as described in the main text. The grey trajectories in the top and bottom panel are thus identical.

the initial condition $z_0 = w$. In components $z_t = x_t + iy_t$, the trajectories of this backward flow satisfy the system of equations

$$\partial_t x_t = -\frac{2x_t}{x_t^2 + y_t^2} - \partial_t \xi(t), \qquad\qquad x_0 = u,$$

$$\partial_t y_t = \frac{2y_t}{x_t^2 + y_t^2}, \qquad\qquad y_0 = v. \qquad (18)$$

The two trajectories shown on the bottom panel in Fig. 3 precisely retrace the trajectories of the forward flow shown on the top panel. This has been achieved by driving the backward evolution (18) by the time reversed noise $\xi(T - t) - \xi(T) \overset{d}{=} \xi(t)$ as compared to the forward evolution. In this case the final point z_T of the trajectory that started at the origin coincides with the tip of the trace $\gamma(T)$ at that time, but the rest of the trajectory does not follow the SLE trace. If we drive the backward flow by an independent

copy of $\xi(t)$, then even the final point z_T will be different from $\gamma(T)$, but in the statistical ensemble z_T and $\gamma(T)$ will have the same distribution.

Now we can introduce the probability distribution function of the process $z_t = x_t + iy_t$ in the physical plane defined by:

$$\rho(x, y, t) = \langle \delta(x_t - x)\delta(y_t - y)\rangle. \tag{19}$$

From Eqs. (3, 18) it follows immediately that $\rho(x, y, t)$ satisfies the following (generalized) Fokker-Planck equation:

$$\partial_t \rho(x, y, t) = \left[\frac{\kappa}{2}\partial_x^2 + c|\partial_x|^\alpha + \partial_x \frac{2x}{x^2 + y^2} - \partial_y \frac{2y}{x^2 + y^2}\right]\rho(x, y, t). \tag{20}$$

Here $|\partial_x|^\alpha$ (sometimes also written as $(-\Delta)^{\alpha/2}$) is the Riesz fractional derivative, which is a singular integral operator whose action is easiest to describe in the Fourier space: if $\tilde{f}(k)$ is the Fourier transform of a function $f(x)$, then the Fourier transform of $|\partial_x|^\alpha f(x)$ is $|k|^\alpha \tilde{f}(k)$.

As we have discussed, at long times the growth is dominated by the stable process in the driving function (3), and we can set $\kappa = 0$. So our main analytical tool is the following Fokker-Planck equation:

$$\partial_t \rho(x, y, t) = \left[c|\partial_x|^\alpha + \partial_x \frac{2x}{x^2 + y^2} - \partial_y \frac{2y}{x^2 + y^2}\right]\rho(x, y, t). \tag{21}$$

Let us discuss the boundary and initial conditions for this equation. The initial condition for the Fokker-Planck equation (21) depends on the initial conditions $x_0 = u$, $y_0 = v$ in the stochastic equations (18). For the distribution of the SLE tip $\gamma(t)$ the appropriate initial conditions are $x_0 = 0$, $y_0 = \epsilon$, where ϵ is an infinitesimal positive number. For the exact Fokker-Planck equation (20) this translates into the initial condition

$$\rho(x, y, 0) = \delta(x)\delta(y - \epsilon). \tag{22}$$

However, for the approximate equation (21) the situation is more subtle. The crossover time $t_0 = O(1)$. For $t < t_0$ the drift in the x direction (towards $x = 0$) dominates over the Lévy term. For $t > t_0$ the opposite is true. A simple picture is then that before t_0 the initial δ function is advected by the drift velocity $2/y$ in the y direction. By the time t_0 it becomes

$$\rho_0(x, y) \equiv \rho(x, y, t_0) = \delta(x)\delta(y - y_0), \qquad y_0 = 2t_0^{1/2} \sim c^{-1/(2-\alpha)}. \tag{23}$$

This is the initial value that we shall assume for our problem. In the following sections we will mostly use the notation $\rho_0(x, y)$, using the explicit expression when necessary.

Let us comment that if we tried to be more careful and included the effects of the Brownian forcing before the crossover time t_0, then the distribution at time t_0 would not only be advected to y_0 but would also broaden to a Gaussian with variance κt_0. This refinement would not change any arguments in the later sections, since all we need there is that the Fourier transform in x of the initial distribution is broader than $e^{-ct|k^\alpha|}$ for long times, see the discussion preceding Eq. (36). This is a good approximation for both the initial distribution (23) or its Gaussian variant for sufficiently long times, and becomes better and better as time increases.

As for the boundary conditions at $y = 0$, we have no need to be very explicit about them, since $\rho(x, y, 0)$ vanishes for $y < y_0$, and our equations of motion (18) represent a situation in which y_t continually increases as t increases, so that $\rho(x, y, t)$ will also vanish for $y < y_0$ at all times $t > 0$.

4   Qualitative description, distance scales

In this section we analyze in qualitative terms the long-time limit of the evolution of the tip $\gamma(t)$, by looking at the consequences of equations (18). According to the discussion in the previous section, $\operatorname{Re} \gamma(t)$ and $\operatorname{Im} \gamma(t)$ have the same joint distribution as x_t and y_t.

For small times, up to the crossover time t_0, the drift term in the Langevin equation dominates over the Lévy noise. Therefore, both x_t and y_t, and $\xi(t)$ as well, grow as $\sqrt{t}$. For larger times, $t \gg t_0$, there are two different characteristic length scales, $X(t)$ and $Y(t)$. In this regime the forcing $\xi(t)$ is dominated by the Lévy process $L_\alpha(t)$. The probability for a total motion $X(t)$ over a time t for this process is described by Eq. (4). Typically the motion is dominated by a single long jump, and the jump has an order of magnitude

$$X(t) \sim (ct)^{1/\alpha}. \tag{24}$$

(This can be understood as rescaled fractional moments $\langle |L_\alpha(t)|^\delta \rangle^{1/\delta}$, see Eq. (6)) Since the typical jumps of $\xi(t)$ become arbitrarily large at long times, x_t also becomes large, and therefore, the drift term in the first equation of (18) becomes negligible. In this limit, x_t behaves like the driving force, and we find

$$t \to \infty : |x_t| \sim X(t) \sim (ct)^{1/\alpha}. \tag{25}$$

The Loewner evolution with Levy flights produces, in general, a forest of (sparse or dense) branching trees, growing form the real axis. The above

12
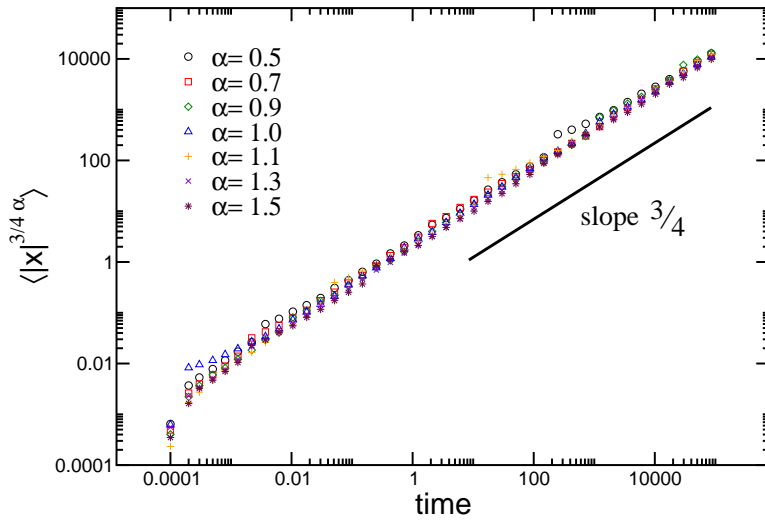
Figure 4: Growth of the Lévy-SLE parallel to the boundary. Here we plot $\langle |x|^{3\alpha/4} \rangle$ for various values of α (Brownian motion is set to zero, $\kappa = 0$). The average follows the predicted behavior $t^{3/4}$. Data collected by averaging realizations of equation (16) for Lévy distributed forcing $c = 1$, time step $\tau = 10^{-4}$; 10000 runs for $\alpha = 0.5, 1.0, 1.3$, 3000 runs for $\alpha = 0.7, 0.9, 1.1, 1.5$. The black line is a guide to the eye with the desired slope. The irregular points observed in some of the curves are due to large jumps in the forcing of individuals runs. Such behavior is expected due to the power law distribution of the jumps in Lévy processes.

relation then tells us how the forest spreads along the real axis with time. This distance is marked out on the plots of trees shown in Figure 2.

Numerical implementation of the Langevin equation (16), details of which are presented in Appendix A.1, confirms these qualitative arguments. Figure 4 compares the estimate of Eq. (25) with numerical calculations of the trace via simulations of Eq. (16). The agreement is excellent.

Next we turn to a typical distance $Y(t)$ in the y coordinate. Figure 2 clearly shows that this characteristic distance is much smaller than $X(t)$. We understand this as follows. If x_t were zero, the second equation in (18) would give $y_t \sim t^{1/2}$. Clearly, any non-zero x_t only slows down the growth of y_t. We then conclude that y_t, and therefore the height of the trees produced by the SLE process cannot grow with time faster than $t^{1/2}$. Since $\alpha < 2$, it means that $\mathrm{Im}\,\gamma(t)$ always grows slower than $\mathrm{Re}\,\gamma(t)$ and they become widely separated at long times. Our major result is that the growing trees spread faster horizontally than they grow vertically. Hence, we have

$$Y(t) \ll X(t). \tag{26}$$

An estimate of the scaling of $Y(t)$ can be obtained from the second equation in (18) where we replace x_t by the Lévy process and average over it using the probability distribution (4). This gives a typical behavior of y_t:

$$\partial_t y_t \approx \int_{-\infty}^{\infty} dx \frac{2y_t}{y_t^2 + x^2} P(x,t) = \int_{-\infty}^{\infty} dk\, e^{-y_t|k| - c|k|^\alpha t}. \tag{27}$$

To estimate the k integral we can drop the term $y_t|k|$ in the exponent, since this quantity is of order $Y(t)/X(t) \ll 1$. Thus we get

$$\partial_t y_t \approx \frac{2\Gamma\left(1 + \frac{1}{\alpha}\right)}{c^{1/\alpha}} t^{-1/\alpha}. \tag{28}$$

The time integration then gives a result that the length scale for the y direction is

$$Y(t) = y_0 + \frac{2}{c^{1/\alpha}} \frac{\Gamma(1 + \frac{1}{\alpha})}{1 - \frac{1}{\alpha}} t^{1 - \frac{1}{\alpha}}. \tag{29}$$

Here y_0 is formally the constant of integration, but it should really be thought of as an adjustable constant inserted to make up for any errors we might have made in doing the integrals. In particular, it takes care of any effects from the early-time region, where we surely do not have the calculation under control.
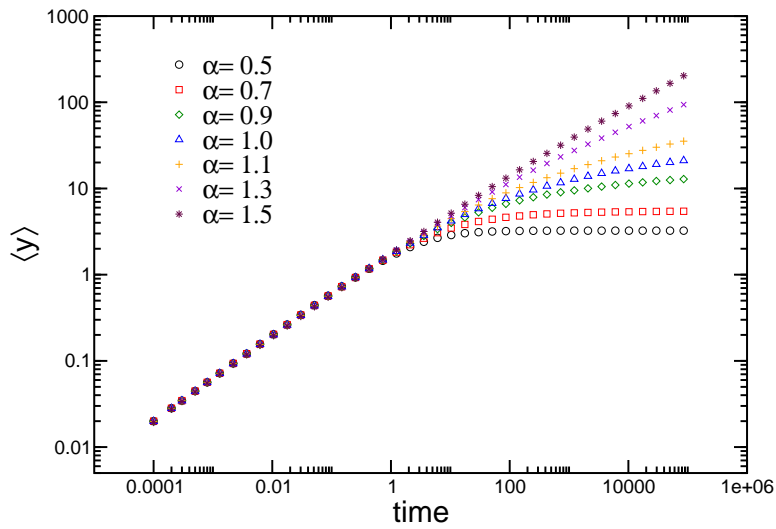
Figure 5: Growth of the Lévy-SLE perpendicular to the boundary. We plot $\langle y \rangle$ for various values of α. Same details as in previous figure. Initially, the trace grows as $\sqrt{t}$ for all values of α. This behavior changes around the characteristic time $t_0 \sim 1$. The height of the trace saturates for $\alpha < 1$, while it grows indefinitely for $\alpha > 1$. This change of behavior demonstrates the global implications of the phase transition at $\alpha = 1$.

The phase transition at $\alpha = 1$ is manifested by a qualitative difference between $\alpha > 1$ and $\alpha < 1$. From (29) we can see that while for $\alpha \geqslant 1$ the average height of the trees grows to infinity as $t^{1-1/\alpha}$, while for $\alpha < 1$ it saturates at a finite value y_∞. Figure 5 provides an illustration of the phase transition at $\alpha = 1$ separating different behaviors. More detailed comparison between our analytical predictions and numerical simulations is provided in the next Section.

5 Solving the FPE

In order to quantify these predictions we need to return our attention to the Fokker-Plank equation (21). If we perform the Fourier transform in x and integrate in time we can find a compact form of this equation, which reads

$$\widetilde{\rho}(k, y, t) = e^{-c|k|^\alpha t}\widetilde{\rho}_0(k, y) - \partial_y \int dk' \int_0^t dt' e^{-y|k'|-c|k|^\alpha(t-t')}\widetilde{\rho}(k - k', y, t')$$

$$+ k \int dk' \int_0^t dt' \operatorname{sgn}(k') e^{-y|k'|-c|k|^\alpha(t-t')}\widetilde{\rho}(k - k', y, t'), \qquad (30)$$

where $\widetilde{\rho}_0(k, y)$ is the Fourier transform of the initial distribution (23). At long times $\rho(x, y, t)$ is spread over the scale $X(t)$ as a function of x. Its Fourier transform $\widetilde{\rho}(k, y, t)$, as a function of k, is significantly non-zero on the scale $X(t)^{-1}$. At the same time, due to the exponential factors $e^{-y|k'|}$, the relevant values of k' in the integrals in Eq. (30) are of the order $y^{-1} \gtrsim Y(t)^{-1}$. The scale $Y(t)^{-1}$ is much larger than the range $X(t)^{-1}$ where ρ is non-zero, hence, when integrating over k' we can use the approximation

$$\widetilde{\rho}(k - k', y, t) \approx \delta(k - k') \int dk'' \widetilde{\rho}(k'', y, t) = 2\pi\rho(0, y, t)\delta(k - k'). \qquad (31)$$

The Fokker-Planck equation then reads:

$$\widetilde{\rho}(k, y, t) = e^{-c|k|^\alpha t}\widetilde{\rho}_0(k, y) - 2\pi \int_0^t dt' e^{-y|k|-c|k|^\alpha(t-t')}\partial_y\rho(0, y, t')$$

$$+ 4\pi|k| \int_0^t dt' e^{-y|k|-c|k|^\alpha(t-t')}\rho(0, y, t'). \qquad (32)$$

This is the main approximation that we will use in order to study the behavior of the Lévy-SLE process at large times.

Notice here that the distribution function ρ, for every x and t, depends only on the initial condition ρ_0 and the history of the distribution at $x = 0$

for earlier times $t' < t$. Therefore, in order to study the probability density function described by the Fokker-Planck equation, we first need to calculate the behavior of this distribution for small x, that is $\rho(0, y, t)$. Then, by substituting in Eq. (32), we can in principle estimate the full distribution. However, in this paper we are mostly interested in the way this process grows in the y direction. Hence, we will first find $\rho(0, y, t)$ which characterizes the growth near $x = 0$, and then obtain the distribution

$$p(y, t) \equiv \int_{-\infty}^{\infty} dx\, \rho(x, y, t) = \widetilde{\rho}(0, y, t) \tag{33}$$

of y's integrated over all x by setting $k = 0$ in (32):

$$p(y, t) = p_0(y) - 2\pi \int_0^t dt'\, \partial_y \rho(0, y, t'). \tag{34}$$

This equation immediately leads to the average $\langle y \rangle$, which is understood as the average over all x:

$$\langle y \rangle = y_0 + 2\pi \int_0^t dt' \int_0^{\infty} dy\, \rho(0, y, t'). \tag{35}$$

Therefore, the distribution and its mean in Eqs. (34) and (35) depend only on the behavior at $x = 0$ at times $t' < t$. This is a direct implication of Eq. (32) and our main approximation (31).

Let us emphasize again that our approximation works in the long time limit. We will assume that we can use approximate expressions in time integrals for all $t > t_0$. Thus, we will treat all time integrals $\int_0^t$ as $\int_{t_0}^t$ + correction. The corrections come from short times, and we cannot extract them from our analysis. They all will be hidden in the terms dependent on the lower limit t_0 of the time integrals. In several cases the lower cut-off at t_0 is necessary to avoid spurious divergencies.

Let us now consider $\rho(0, y, t)$. A closed equation for this quantity results from integrating Eq. (32) over k. To do this we observe that in the first term (the initial value at $t = 0$) for the relevant values of k the function $\widetilde{\rho}_0(k, y)$ is much broader in k than $e^{-c|k|^{\alpha} t}$ at long times. Hence, in the integral over k we can replace $\widetilde{\rho}_0(k, y)$ by its value at $k = 0$. Then it follows that

$$\rho(0, y, t) = \frac{\widetilde{\rho}_0(0, y)}{2\pi X(t)} - \int_0^t dt'\, \frac{\partial_y \rho(0, y, t')}{X(t - t', y)} - 2 \int_0^t dt'\, \rho(0, y, t') \partial_y \frac{1}{X(t - t', y)},$$
$$\tag{36}$$

where the scale $X(t, y)$ is defined as

$$\frac{1}{X(t, y)} = \int_{-\infty}^{\infty} dk\, e^{-c|k|^{\alpha}t - y|k|}, \tag{37}$$

and

$$X(t) = X(t, y = 0) = \frac{c^{1/\alpha}}{2\Gamma\left(1 + \frac{1}{\alpha}\right)} t^{1/\alpha}. \tag{38}$$

Equation (36) is easily solved after performing the Laplace transformation in time t. For the transform

$$\rho(0, y, \lambda) = \int_0^{\infty} dt\, e^{-\lambda t} \rho(0, y, t) \tag{39}$$

we obtain an ordinary differential equation

$$\partial_y \rho(0, y, \lambda) + \frac{1 + 2\partial_y K(\lambda, y)}{K(\lambda, y)} \rho(0, y, \lambda) = \frac{K(\lambda)}{2\pi K(\lambda, y)} \widetilde{\rho}_0(0, y), \tag{40}$$

where

$$K(\lambda, y) = \int_0^{\infty} dt\, \frac{e^{-\lambda t}}{X(t, y)} = \int_{-\infty}^{\infty} dk\, \frac{e^{-y|k|}}{\lambda + c|k|^{\alpha}}, \tag{41}$$

and $K(\lambda) = K(\lambda, 0)$. Using the initial condition $\widetilde{\rho}_0(0, y) = \delta(y - y_0)$, the straightforward solution of Eq. (40) is

$$\rho(0, y, \lambda) = \frac{K(\lambda)}{2\pi} \frac{K(\lambda, y_0)}{K^2(\lambda, y)} \exp\left(-\int_{y_0}^{y} \frac{dy'}{K(\lambda, y')}\right). \tag{42}$$

The inverse Laplace transform of this solution gives $\rho(0, y, t)$.

Notice that (42) is valid only for $y > y_0$. Since our approximations only work at long times, we expect our solution to give good results for $y \gg y_0$. The approximations will usually result in the necessity to introduce a fitting parameter (called "correction" in the discussion after Eq. (35)) in the time evolution of averages for the process. Moreover, there is an upper cut-off that stems from the Langevin equation and the fact that y cannot grow faster than $t^{1/2}$ (see previous section). Since we used this fact while making the approximations that lead to Eq. (32), the range of validity of our solution is $y_0 \ll y \ll t^{1/2}$.

In the following we will analyze the properties of the distributions $\rho(0, y, t)$ and $p(y, t)$ in three separate cases $\alpha > 1$, $\alpha = 1$ and $\alpha < 1$. For each case

we will repeat the following steps: first we calculate $\rho(0, y, t)$ from Eq. (42), then, by substituting this solution into Eq. (34), we will calculate the average height $\langle y \rangle$ and the distribution $p(y, t)$. In these calculations we need approximate expressions for the function $K(\lambda, y)$. These expressions are derived in Appendix A.2.

5.1 Results for $\alpha > 1$

In this case we can use the approximation (86) from Appendix A.2 for $K(\lambda)$ and $K(\lambda, y)$. Eq. (42) then gives

$$\rho(0, y, \lambda) \approx \frac{1}{2\pi} \exp\left(-\frac{1}{A}\lambda^{1-1/\alpha}y\right), \qquad A = \frac{2\pi}{\alpha c^{1/\alpha} \sin\frac{\pi}{\alpha}}. \qquad (43)$$

To calculate the time dependence of the distribution we take the inverse Laplace transform:

$$\rho(0, y, t) \approx \frac{1}{2\pi t} \int_{a-i\infty}^{a+\infty} \frac{d\lambda}{2\pi i} e^{\lambda t - \lambda^{1-1/\alpha}y/A}. \qquad (44)$$

As usual, the integration contour in the last equation goes along a vertical line $\mathrm{Re}\,\lambda = a$, where a should be greater than the real part of any singularity of the integrand. Changing the integration variable to λt we obtain that answer which, apart from the overall prefactor $1/t$, has acquired the form of a scaling function:

$$\rho(0, y, t) \approx \frac{1}{2\pi t}F(\hat{y}), \qquad \hat{y} \equiv \frac{y}{Y(t)}, \qquad Y(t) = \frac{2}{c^{1/\alpha}}\frac{\pi}{\alpha \sin\frac{\pi}{\alpha}}t^{1-\frac{1}{\alpha}}, \qquad (45)$$

$$F(\hat{y}) = \int \frac{d\lambda}{2\pi i}e^{\lambda - \lambda^{1-1/\alpha}\hat{y}}. \qquad (46)$$

Since the scaling function $F(\hat{y})$ depends only on the combination $yt^{-1+1/\alpha}$, its derivatives with respect to y and t are related:

$$\partial_y F(\hat{y}) = -\frac{\alpha}{\alpha - 1}\frac{t}{y}\partial_t F(\hat{y}). \qquad (47)$$

The integrand in Eq. (46) contains a branch cut which we choose to run along the negative real axis. The integration contour can be deformed to go from $-\infty$ to 0 along the lower side of the cut, and then from 0 to $-\infty$ along the upper side. This leads to the final answer for the scaling function $F(\hat{y})$:

$$F(\hat{y}) = \frac{1}{\pi} \int_0^\infty d\lambda\, e^{-\lambda - |\cos\frac{\pi}{\alpha}|\lambda^{1-1/\alpha}\hat{y}} \sin\left(\sin\frac{\pi}{\alpha}\lambda^{1-1/\alpha}\hat{y}\right). \qquad (48)$$
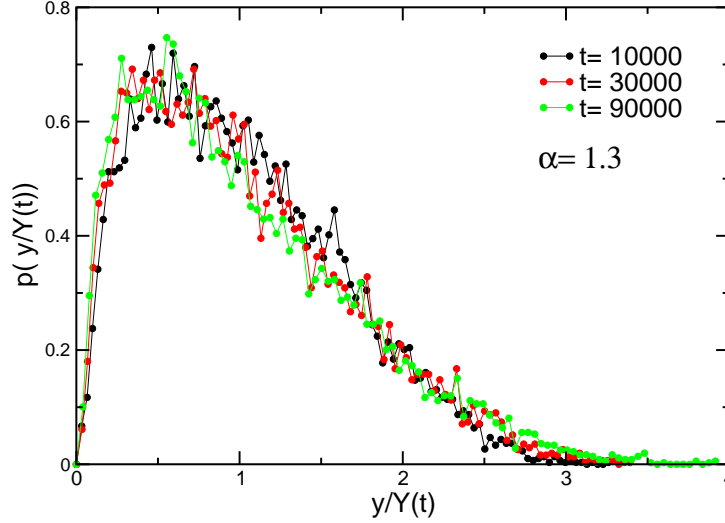
Figure 6: The distribution of heights scales as $y/Y(t)$, where $Y(t)$ is given by Eq. (45) for $\alpha = 1.3$. The distribution is shown at three different times (black, red and green curves), all within the limiting region of large times where asymptotic behavior $y \propto t^{1-1/\alpha}$ holds.

The overall prefactor $1/t$ in $\rho(0,y,t)$ can be understood as follows. The distribution $\rho(x,y,t)$ at long times spreads in the x direction up to scale $X(t)$, and in the y direction up to scale $Y(t)$. The total area "covered" by the distribution scales with time as $X(t)Y(t) \propto t$. Therefore, at the particular value $x = 0$ the density $\rho(0,y,t)$ decays with time as $1/t$. However, if we are looking at the distribution of the y coordinate for $x = 0$, and its moments $\langle y^n \rangle$, we should divide $\rho(0,y,t)$ by the normalization

$$\int_0^\infty dy\, \rho(0,y,t) = \frac{Y(t)}{2\pi t \Gamma\left(1 - \frac{1}{\alpha}\right)}. \tag{49}$$

The normalized distribution is then

$$\rho_n(0,y,t) \approx \frac{\Gamma\left(1 - \frac{1}{\alpha}\right)}{Y(t)} F(\hat{y}). \tag{50}$$

Moreover, the integrated distribution $p(y,t)$ exhibits the same scaling as $\rho(0,y,t)$. Indeed, using the relation (47) in Eq. (34) we obtain:

$$p(y,t) = p_0(y) + \frac{1}{Y(t)} \frac{\alpha}{\alpha - 1} \frac{1}{\hat{y}} F(\hat{y}). \tag{51}$$

20
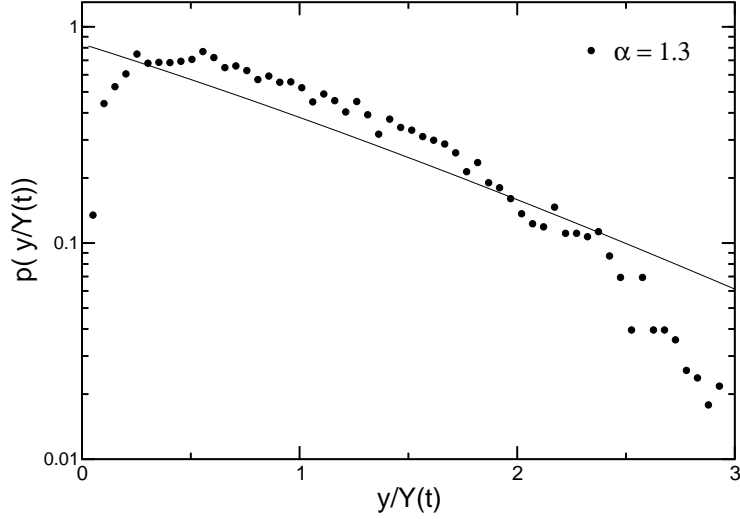
Figure 7: The distribution $p(y,t)$ as a function of $y/Y(t)$. The theoretical prediction Eq. (51) (solid curve) and the numerical distribution (black dots) are different, however, they have a similar dependence on y for the values where we believe the solution is valid, $t_0^{1/2} \ll y \ll t^{1/2}$. Here, $Y(t) = 50$, $t^{1/2} \approx 300$ and $t_0^{1/2} \approx 1$, so the region of validity of Eq. (51) in the scaled variable is $0.02 \ll y/Y(t) \ll 6$. This explains the disagreement between the theory and the numerics for $y/Y(t) > 2$. Also, for small values of $y/Y(t)$ where we should not trust Eq. (51), the theory still gives a significant weight to the distribution $p(y,t)$. This is, presumably, the reason for the discrepancy between the numerics and the theory in the range $y/Y(t) < 2$.

Fig. 6 shows the scaling collapse of the numerically calculated distributions $p(y,t)$ for $\alpha = 1.3$ and three different times. We see that, indeed, $p(y,t)$ is a scaling function of $y/Y(t)$ in agreement with our predictions.

We can calculate the asymptotics of the function $F(\hat{y})$. For small values of $\hat{y}$ we can neglect the term with $\hat{y}$ in the exponential in Eq. (46), as well as replace the sine function under the integral by its (small) argument:

$$F(\hat{y} \ll 1) \approx \frac{\alpha - 1}{\alpha} \frac{1}{\Gamma(\frac{1}{\alpha})} \hat{y}. \tag{52}$$

For large $\hat{y}$ we need to use the steepest descent method for the contour integral in Eq. (46), which results in

$$F(\hat{y} \gg 1) \approx \left(\frac{\alpha}{2\pi}\right)^{1/2} \left(\frac{\alpha - 1}{\alpha} \hat{y}\right)^{\alpha/2} \exp\left[-\frac{1}{\alpha - 1}\left(\frac{\alpha - 1}{\alpha} \hat{y}\right)^{\alpha}\right]. \tag{53}$$

21
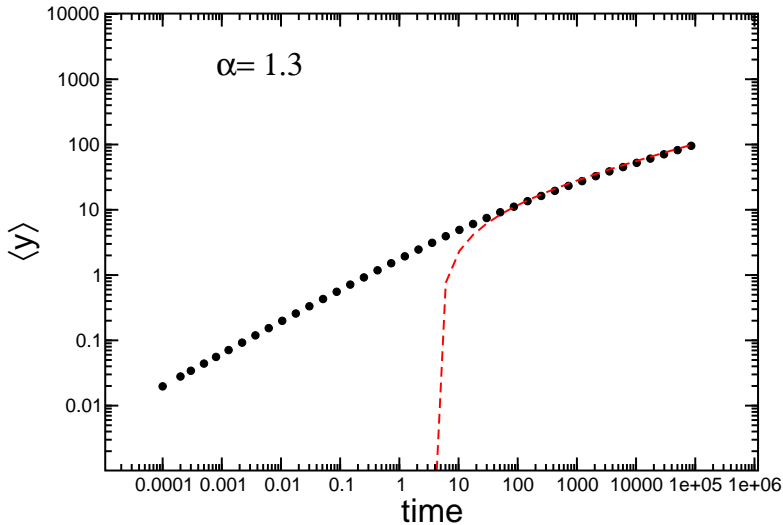
Figure 8: The average height $\langle y \rangle$ for SLE driven by Lévy flights with $\alpha = 1.3$ grows as a power-law $t^{1-1/\alpha}$. The red dashed line is a fit to Eq. (54) for $t > 1$, where we only vary the parameter y_0.

We have to remember that we can only trust this result for $y_0 \ll y \ll t^{1/2}$.

Figure 7 shows a comparison between the numerical data and the theoretical prediction of Eq. (51) for the distribution $p(y, t)$. While the overall dependence on y is similar between the two, we would obtain a better fit for $y_0 \ll y \ll t^{1/2}$ if we redistributed the weight outside this region to the range were Eq. (51) is valid.

Next, we will calculate the time evolution of the average height of the growing trees $\langle y \rangle$ from Eqs. (35, 49):

$$\langle y \rangle = y_0 + \frac{1}{\Gamma(1 - \frac{1}{\alpha})} \int_0^t dt' \frac{Y(t')}{t'} = y_0 + \frac{2}{c^{1/\alpha}} \frac{\Gamma(1 + \frac{1}{\alpha})}{1 - \frac{1}{\alpha}} t^{1 - \frac{1}{\alpha}}. \qquad (54)$$

Here, all short time contributions are included in y_0. This nicely fits the numerics, see Fig. 8, and reproduces the result (29) of the simple argument using the Langevin equation.

We also want to compare the distribution at $x = 0$ to the distribution averaged over all x. We calculate the average value $\langle y \rangle^0$ (the superscript indicates that this average is calculated at $x = 0$) from the distribution (50):

$$\langle y \rangle^0 = \frac{4}{\alpha c^{1/\alpha}} \left| \cos \frac{\pi}{\alpha} \right| \Gamma\left(1 - \frac{1}{\alpha}\right) \Gamma\left(\frac{2}{\alpha} - 1\right) t^{1 - 1/\alpha}. \qquad (55)$$

22
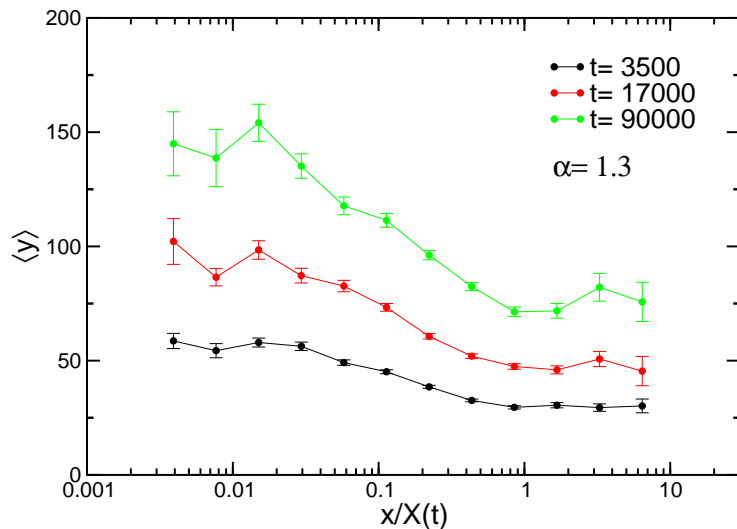
Figure 9: Average height of the trace $y = \operatorname{Im} \gamma(t)$ as a function of $x/(ct)^{1/\alpha}$ for SLE driven by Levy flights with $\alpha = 1.3$. y data are bined logarithmically. Here, $(ct)^{1/\alpha} = 1827.15$, 6217.82, 21156.6 for the three values of time. The average height close to $x = 0$ is 2 times bigger than the height at large x and roughly 1.4 times higher than the global average $\langle y \rangle$. The theoretically predicted value of the ratio between the height at $x = 0$ and the average is 1.9 (Eq. (56)). This discrepancy is most probably due to a finite time effect and the limited amount of data close to $x = 0$.

23

The ratio of the two averages (neglecting y_0) is

$$\frac{\langle y \rangle^0}{\langle y \rangle} = \frac{1}{\pi} \left| \sin \frac{2\pi}{\alpha} \right| \Gamma\left(1 - \frac{1}{\alpha}\right) \Gamma\left(\frac{2}{\alpha} - 1\right) \Gamma\left(2 - \frac{1}{\alpha}\right). \tag{56}$$

This tends to 2 as $\alpha \to 1$ from above, and to $\pi/2$ as $\alpha \to 2$ from below. We observe similar behavior in our numerical results, where the average of y at $x = 0$ is higher than the overall average (Fig. 9). However, the ratio (56) is not matched exactly. Presumably, this is because we do not have enough data close to $x = 0$ and we cannot reach long enough times in order for the various constants (like y_0) to be negligible, so that Eq. (56) is accurate.

5.2 Results for $\alpha = 1$

Now we use the approximations (79, 84) from Appendix A.2 in Eq. (42). The resulting expression for $\rho(0, y, \lambda)$ is difficult to analyze without further approximations. We will evaluate it as well as its inverse Laplace transform with logarithmic accuracy, which amounts to three assumptions. First, we assume that all the logarithms that appear are large compared to constants of order one such as π, c, etc, which will be neglected. Secondly, the logarithms are assumed to be small compared to power laws for large arguments: $\ln t \ll t$. Finally, the logarithms are slow functions as compared to power laws and exponentials, and in integrals can be replaced by their values at the typical scale of variation of the fastest function under the integral. All subsequent equations in this section will be obtained with logarithmic accuracy using these assumptions.

First we have

$$\rho(0, y, \lambda) \approx \frac{1}{2\pi} \frac{\ln \frac{1}{\lambda t_0} \ln \frac{c}{\lambda y_0}}{\ln^2 \frac{c}{\lambda y}} \exp\left(-\frac{c}{2} \frac{y}{\ln \frac{c}{\lambda y}}\right). \tag{57}$$

The time dependence now follows from the inverse Laplace transform, using the same contour integral described in the previous section:

$$\rho(0, y, t) \approx \frac{1}{2\pi^2 t} \int_0^\infty d\lambda \frac{\ln \frac{t}{\lambda t_0} \ln \frac{ct}{\lambda y_0}}{\ln^2 \frac{ct}{\lambda y}} \sin\left(\frac{\pi}{2} \frac{cy}{\ln^2 \frac{ct}{\lambda y}}\right) \exp\left(-\lambda - \frac{c}{2} \frac{y}{\ln \frac{ct}{\lambda y}}\right). \tag{58}$$

The integral of this expression over y

$$\int_0^\infty dy \, \rho(0, y, t) \approx \frac{1}{\pi ct} \frac{\ln \frac{t}{t_0} \ln \frac{ct}{y_0}}{\ln^2 \left(\frac{c^2 t}{2}\right)} \tag{59}$$

24
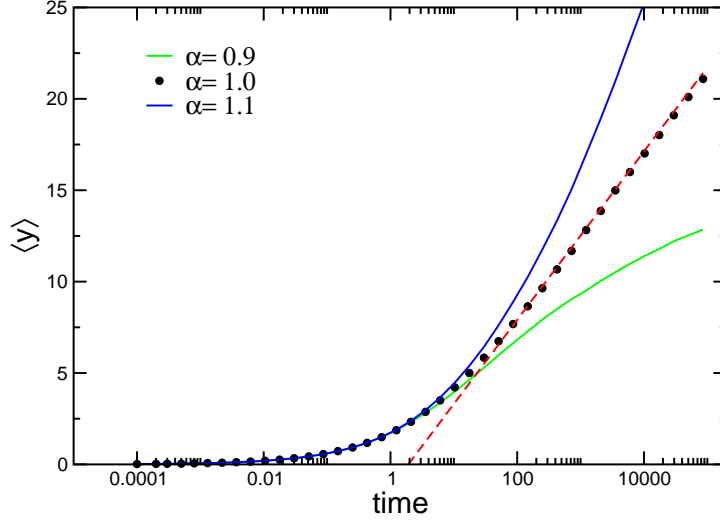
Figure 10: The average height $\langle y \rangle$ for SLE driven by Lévy flights $\alpha = 1.0$ grows logarithmically with time. The red dashed line is a one parameter fit for $t > 10$ to the predicted function $A + \frac{2}{c} \ln t$.

leads to a normalized distribution at $x = 0$:

$$
\rho_n(0, y, t) \approx \frac{c}{2\pi} \frac{\ln^2 \left(\frac{c^2 t}{2} \right)}{\ln \frac{t}{t_0} \ln \frac{ct}{y_0}}
$$
$$
\times \int_0^\infty d\lambda \frac{\ln \frac{t}{\lambda t_0} \ln \frac{ct}{\lambda y_0}}{\ln^2 \frac{ct}{\lambda y}} \sin \left(\frac{\pi}{2} \frac{cy}{\ln^2 \frac{ct}{\lambda y}} \right) \exp \left(- \lambda - \frac{c}{2} \frac{y}{\ln \frac{ct}{\lambda y}} \right).
$$

(60)

The mean value of the height of trees near $x = 0$ follows from $\rho_n(0, y, t)$ using the same arguments as before:

$$
\langle y \rangle^0 \approx \frac{4}{c} \ln \frac{c^2 t}{2}.
$$

(61)

The average height (over all x) is also found easily from Eq. (35):

$$
\langle y \rangle = y_0 + \frac{2}{c} \int_{t_0}^t \frac{dt'}{t'} \frac{\ln \frac{t'}{t_0} \ln \frac{ct'}{y_0}}{\ln^2 \left(\frac{c^2 t'}{2} \right)} \approx \frac{2}{c} \ln t + \text{ const.}
$$

(62)

As shown in Fig. 10 this is in good agreement with the numerics. The ratio of the two averages in the long time limit is $\langle y \rangle^0 / \langle y \rangle = 2$, consistent with the limit $\alpha \to 1$ of Eq. (56).

25

The asymptotics of the distribution $\rho_n(0, y, t)$ for small and large values of $y/\ln ct$ can be found similar to the case $\alpha > 1$:

$$\rho_n(0,y,t) \approx \begin{cases} \dfrac{c^2}{4} \dfrac{\ln^2 \frac{c^2 t}{2}}{\ln^4 \frac{ct}{y}} y, & y_0 \ll y \ll \ln ct, \\[3ex] \dfrac{c^{3/2}}{4\pi^{1/2}} \dfrac{\ln^2 \frac{c^2 t}{2}}{\ln \frac{t}{t_0} \ln \frac{ct}{y_0}} \dfrac{\ln \frac{8t}{ct_0 y} \ln \frac{8t}{y_0 y}}{\ln^3 \frac{8t}{y^2}} y^{1/2} \exp\Big(- \dfrac{cy}{2\ln \frac{8t}{y^2}}\Big), & \ln ct \ll y \ll t^{1/2}. \end{cases}$$

(63)

Finally, using Eq. (34), we get an expression for the integrated distribution:

$$p(y,t) \approx p_0(y) + \frac{c}{2\pi} \ln \frac{t}{t_0} \int_0^\infty d\lambda \frac{\ln \frac{t}{\lambda t_0} \ln \frac{ct}{\lambda y_0}}{\ln^3 \frac{ct}{\lambda y}} \sin\Big(\frac{\pi}{2} \frac{cy}{\ln^2 \frac{ct}{\lambda y}}\Big) \exp\Big(-\lambda - \frac{c}{2} \frac{y}{\ln \frac{ct}{\lambda y}}\Big).$$

(64)

The asymptotics of these expression follow as before:

$$p(y,t) - p_0(y) \approx \begin{cases} \dfrac{c^2}{4} \dfrac{\ln^2 \frac{t}{t_0} \ln \frac{ct}{y_0}}{\ln^5 \frac{ct}{y}} y, & y_0 \ll y \ll \ln ct, \\[3ex] \dfrac{c^{3/2}}{4\pi^{1/2}} \dfrac{\ln \frac{t}{t_0} \ln \frac{8t}{ct_0 y} \ln \frac{8t}{y_0 y}}{\ln^4 \frac{8t}{y^2}} y^{1/2} \exp\Big(- \dfrac{cy}{2\ln \frac{8t}{y^2}}\Big), & \ln ct \ll y \ll t^{1/2}. \end{cases}$$

(65)

5.3   Results for $\alpha < 1$

In this case we use the approximation (87) from Appendix A.2 leading to

$$\rho(0, y, \lambda) \approx N K(\lambda) y^{2-2\alpha} \exp\Big(- \frac{y^{2-\alpha}}{C(2-\alpha)}\Big),$$

(66)

$$C = \frac{2}{c}\Gamma(1-\alpha), \qquad N = \frac{y_0^{\alpha-1}}{2\pi C}.$$

(67)

The inverse Laplace transform of this expression gives the leading approximation

$$\rho(0, y, t) \approx \frac{N}{X(t)} y^{2-2\alpha} \exp\Big(- \frac{(1-\alpha)c}{2\Gamma(3-\alpha)} y^{2-\alpha}\Big).$$

(68)

The obtained result depends on time only through the overall factor $X^{-1}(t)$. We can understand this as follows. The distribution $\rho(x, y, t)$ at
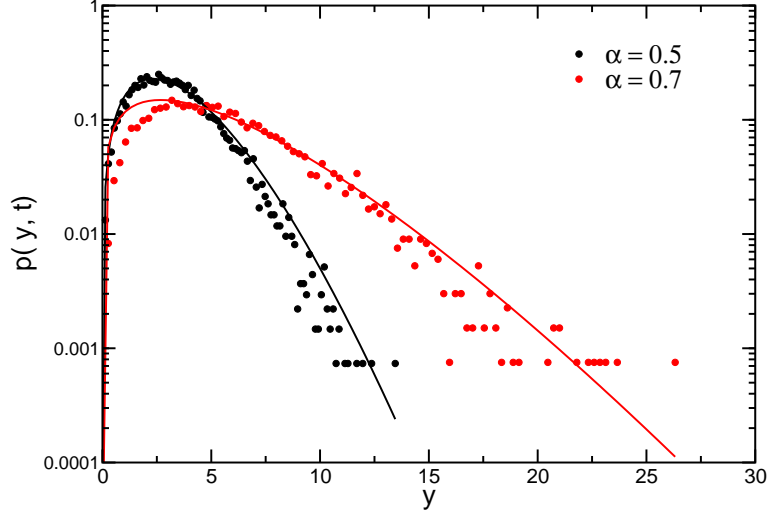
Figure 11: Distribution fits for $\alpha < 1$. We compare the numerically calculated distribution $p(y,t)$ to the theoretical curve for ρ_∞ given by Eq. (69) with one free parameter for normalization. We claim that $p(y,t) = \rho_\infty(0,y)$ for $y_0 \ll y \ll t^{1/2}$ where our solution is valid.

long times spreads in the x direction up to the scale $X(t)$ but becomes stationary in the y direction. Therefore, at the particular value $x = 0$ the density $\rho(0,y,t)$ decays with time as $X^{-1}(t)$. However, if we are looking at the distribution of the y coordinate for $x = 0$, we should normalize Eq. (68) which gives the truly stationary distribution (normalized by the appropriate choice of N_1)

$$\rho_\infty(0,y) \approx N_1 y^{2-2\alpha} \exp\Big(- \frac{(1-\alpha)c}{2\Gamma(3-\alpha)} y^{2-\alpha} \Big), \qquad (69)$$

in agreement with numerics, see Fig. 11, where we actually observe that the integrated distribution $p(y,t)$ coincides with $\rho_\infty(0,y)$ at long times.

The stationary distribution (69) allows us to calculate the average saturated height of the trees:

$$y_\infty = \int_0^\infty dy\, y \rho_\infty(0,y) = \Big(\frac{2\Gamma(3-\alpha)}{1-\alpha} \Big)^{1/(2-\alpha)} \Gamma^{-1}\Big(\frac{3-2\alpha}{2-\alpha} \Big) c^{-1/(2-\alpha)}. \quad (70)$$

This is in very good agreement with the numerically calculated values shown in Fig. 12.

27
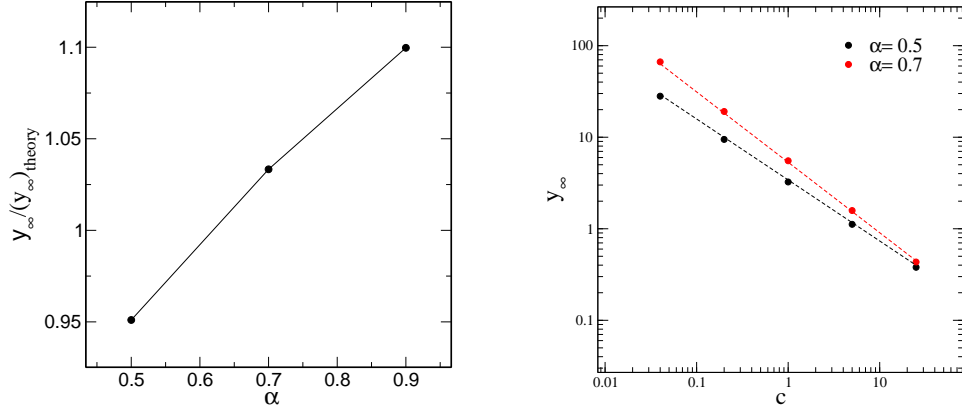
Figure 12: (Left) The ratio of the numerically calculated over the theoretically predicted value of the saturated height y_∞ for $\alpha < 1$. (Right) The saturated height of the trees vs. the strength. The dashed lines are the theoretical values for y_∞, Eq. (70).
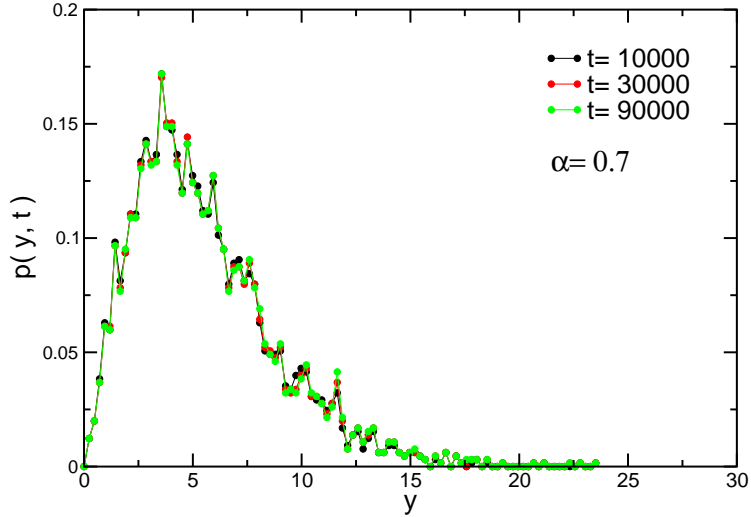
Figure 13: Distribution of heights averaged over all x for SLE driven only by Lévy flights and $\alpha = 0.7$. The distribution is shown at three different times (black, red and green curves), corresponding at the limit of large time. We see how the distribution of the height of trees is stationary.
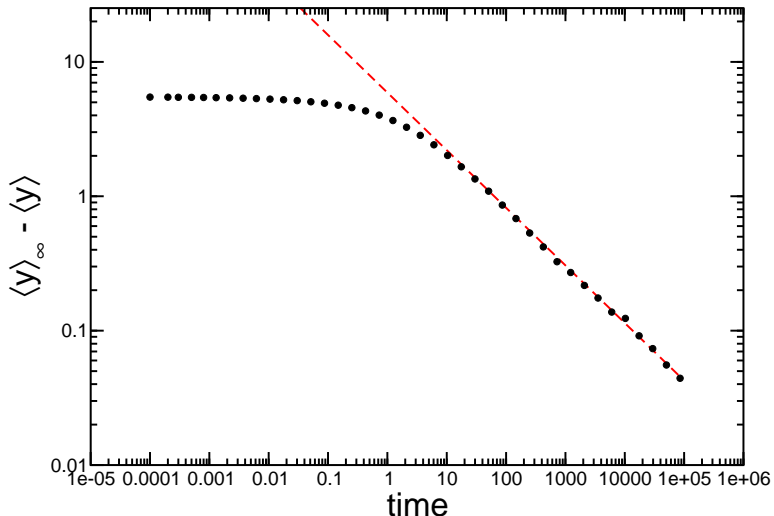
Figure 14: The average height $\langle y \rangle$ for SLE driven by Lévy flights $\alpha = 0.7$ saturates to $\langle y \rangle_\infty$ as $t^{1-1/\alpha}$. The red dashed line is the analytic result, Eq. (71), with the value of $D = \frac{2\Gamma(1+1/\alpha)}{c^{1/\alpha}(1-1/\alpha)}$ obtained in Eq. (29). $\langle y \rangle_\infty$ was calculated from the two numerical points of y for the largest times.

Let us discuss now the integrated distribution $p(y, t)$ and its mean $\langle y \rangle$. Unfortunately, in the present case ($\alpha < 1$), the Eqs. (34) and (35) do not give reliable results simply because the apparent distribution and saturation height are very sensitive to the lower limit t_0, and the results are of the same order as the initial conditions at t_0. Analytically, we can see that the distribution $p(y, t)$ becomes stationary as $t \to \infty$, even though we cannot determine $p(y, \infty)$. The time independence of the distribution $p(y, t)$ at long times is checked numerically in Fig. 13. Numerics presented in Fig. 11 indicate that $p(y, t) = \rho_\infty(0, y)$ (see Eq. (69)) for the appropriate range $y_0 \ll y \ll t^{1/2}$, and we will discuss why this is true below.

We can also see that the way the average tree height approaches its limiting value is given by the power law

$$\langle y \rangle = \langle y \rangle_\infty - D c^{-1/\alpha} t^{1-1/\alpha}. \tag{71}$$

We have previously calculated D in Eq. (29) using the Langevin formulation of the process. This result agrees well with numerics, as demonstrated in Fig. 14.

We can argue that $\langle y \rangle_\infty = y_\infty$ and that $p(y, \infty) = \rho_\infty$, if we return to the initial description of the process seen as SLE trees growing forward in

29
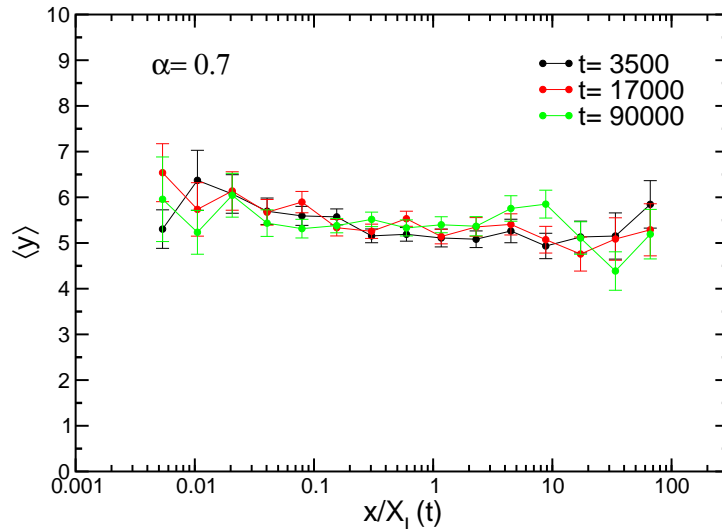
Figure 15: Average height of the trace $y = \text{Im}\,\gamma(t)$ as a function of $x/(ct)^{1/\alpha}$ for SLE driven by Levy flights with $\alpha = 0.7$. y data are binned logarithmically and the average of every bin is plotted. $(ct)^{1/\alpha} = 2.9\ 10^5, 2.8\ 10^6, 2.75\ 10^7$.

time [1]. For $\alpha < 1$ the jumps of the Lévy process are large and we know that any new tree is most likely to grow starting from the real axis. The trees are sparse and the new tree will grow isolated from its neighbors, hence it will be identical to any other tree, including the trees that grow close to the origin at $x = 0$. Therefore, we expect the distribution of y's at $x = 0$ to be identical to the distribution at any other x. Numerics also support this argument. In Fig. 15 we observe that the average height of the trees is practically independent of the value of x. Also, in Fig. 11 we compare $p(y, \infty)$ and ρ_∞ while in Fig. 12 we show that $\langle y \rangle_\infty = y_\infty$.

6 Conclusions

In this paper we have analyzed the global properties of growth in the complex plain described by a generalized stochastic Loewner evolution driven by a symmetric stable Lévy process $L_\alpha(t)$, introduced in our previous paper [1]. The phase transition at $\alpha = 1$ whose implications for local properties of growth were the subject of Ref. [1], also manifests itself on the whole plane resulting in a rich scaling behavior.

We have used a Fokker-Planck equation to study the joint distribution $\rho(x, y, t)$ for the real and imaginary parts of the tip of the growing trace. The presence of the Lévy flights in the driving force imposes very different dynamics in the x and y directions. While in the x direction the process spreads similarly to the Lévy forcing $x \sim X(t) \sim t^{1/\alpha}$, the SLE dictates $y \ll X(t)$, for all values of α. This separation of the horizontal and vertical scales in the process allows us to make sensible approximations and explore geometric properties of the stochastic growth in all phases, $\alpha < 1$, $\alpha = 1$, and $\alpha > 1$, both qualitatively and quantitatively.

For $\alpha < 1$, the vertical growth saturates at a finite height y_∞. In terms of the picture presented in [1], long jumps occur often so that new trees grow isolated and there is a small chance that the trace grows on an already existing tree.

For $\alpha > 1$, the average height of the process grows as a power law $t^{1-1/\alpha}$ with time. New trees grow close to old ones, so that when the process returns to a previously visited part of the real axis it will have to grow on top of already existing trees. Eventually the trace will grow past any point on the plane.

At the boundary between the two phases, $\alpha = 1$, the height of the process grows logarithmically with time.

7   Acknowledgements

A   Appendices

A.1   Numerical calculations

The interpretation of equation (16) is very helpful to our calculations. z_t and the tip of the trace have the same distribution. This allows, instead of calculating the trace $\gamma(t)$ for every time t and noise realization $(O(n^2))$, to efficiently collect statistics for the position of the tip by integrating the Langevin equation (16) $(O(n))$.

Following Ref. [1] we approximate $\xi(t)$ by a piecewise constant function

with jumps appropriately distributed: $\xi(t) = \xi_j$ for $(j-1)\tau < t < j\tau$. For such a driving function the process z_t in Eq. (16) can then be calculated numerically as an iteration process of infinitesimal maps [24] starting from the condition $z = 0$ as follows:

$$z_n = z(n\tau) = f_n \circ f_{n-1} \ldots \circ f_1(0) - \xi_n. \tag{72}$$

The infinitesimal conformal map f_n at each time interval n is defined by:

$$f_n(z) = w_n^{-1}(z) = \sqrt{(z-\xi_n)^2 - 4\tau} + \xi_n \tag{73}$$

The value of ξ_n is randomly drawn from the appropriate distribution. The number of steps necessary to produce an SLE trace up to step n grows only as $O(n)$. All numerical results in the next section have been calculated using the average of Eq. (73) over many noise realizations.

The trace can also be produced directly [1], as $g^{-1}(\xi(t), t)$, in which case we approximate

$$\gamma_j = \gamma(j\tau) = f_1 \ldots \circ f_{n-1} \circ f_n(\xi_n). \tag{74}$$

However, the number of steps in this method grows as $O(n^2)$. We used this method to verify that numerically calculated z and γ have identical distributions. Eq. (74) was also used to calculate the traces shown in Fig. 2.

Here, we will assume $\kappa = 0$ for simplicity, that is, the driving force is pure Lévy flights $\xi(t) = c^{1/\alpha} L_\alpha(t)$. The addition of a Brownian motion will not affect our conclusions. For all realizations of the Lévy-SLE process we take $c = 1$ and $\tau = 10^{-4}$ unless otherwise noted.

A.2 Asymptotics for $K(\lambda, y)$

Let us consider (we need to use the lower cut off t_0 here to have a convergent result for $\alpha < 1$)

$$
K(\lambda) = \int_{t_0}^\infty dt\, \frac{e^{-\lambda t}}{X(t)} = \frac{2\Gamma\left(1 + \frac{1}{\alpha}\right)}{c^{1/\alpha}} \int_{t_0}^\infty dt\, t^{-1/\alpha} e^{-\lambda t}
$$
$$
= \begin{cases} \dfrac{2\Gamma\left(1 + \frac{1}{\alpha}\right)}{c^{1/\alpha}} \lambda^{-1+1/\alpha} \Gamma\left(1 - \frac{1}{\alpha}, \lambda t_0\right), & \alpha \neq 1, \\[2mm] \dfrac{2}{c} E_1(\lambda t_0), & \alpha = 1, \end{cases} \tag{75}
$$

where $\Gamma(a, x)$ is the incomplete gamma function, and $E_1(x)$ is the exponential integral. Since λ has the dimension and the meaning of frequency, and

we are interested in $t \gg t_0$, we will only need the small argument asymptotics of these functions:

$$\Gamma(a,x) \approx \Gamma(a) - \frac{x^a}{a}, \qquad E_1(x) \approx -\ln x, \qquad x \ll 1, \qquad (76)$$

This gives for $\lambda t_0 \ll 1$

$$K(\lambda) \approx A\lambda^{-1+1/\alpha} + Bt_0^{1-1/\alpha}, \qquad \alpha \neq 1, \qquad (77)$$

$$A = \frac{2\pi}{\alpha c^{1/\alpha} \sin \frac{\pi}{\alpha}}, \qquad B = \frac{2}{c^{1/\alpha}} \frac{\alpha}{1-\alpha} \Gamma\left(1 + \tfrac{1}{\alpha}\right), \qquad (78)$$

$$K(\lambda) \approx \frac{2}{c} \ln \frac{1}{\lambda t_0}, \qquad \alpha = 1, \qquad (79)$$

For $\alpha > 1$ we can set $t_0 = 0$ and obtain

$$K(\lambda) = A\lambda^{-1+1/\alpha}, \qquad \alpha > 1 \qquad (80)$$

and for $\alpha < 1$ we can set $\lambda = 0$:

$$K(0) = Bt_0^{1-1/\alpha}, \qquad \alpha < 1. \qquad (81)$$

We now turn to the Laplace transform $K(\lambda, y)$:

$$K(\lambda, y) = 2 \int_0^\infty dk \, \frac{e^{-yk}}{\lambda + ck^\alpha}. \qquad (82)$$

Since in the Laplace transform the important values of λ are the inverse typical time scales, this means that the relevant asympotics of $K(\lambda, y)$ are those with $\lambda y^\alpha/c \ll 1$. The opposite case of $\lambda y^\alpha/c \gg 1$ corresponds to short times, where our basic approximation is invalid. So from now on we will focus on the limit $\lambda y^\alpha/c \ll 1$.

This integral can be evaluated exactly in a number of cases. First, when $y = 0$, the integral converges for $\alpha > 1$ and gives the same expression as $K(\lambda)$ in Eq. (80). Secondly, for $\lambda = 0$ the integral converges (for $y > 0$) for $\alpha < 1$ and gives then

$$K(0, y) = \frac{2}{c} \int_0^\infty dk \, k^{-\alpha} e^{-yk} = Cy^{\alpha-1}, \qquad C = \frac{2}{c}\Gamma(1-\alpha). \qquad (83)$$

All the constants A, B, and C defined above diverge as $1/(\alpha - 1)$ as $\alpha \to 1$. Finally, for $\alpha = 1$ we get

$$K(\lambda, y) = \frac{2}{c} e^{\lambda y/c} E_1\left(\tfrac{\lambda y}{c}\right) \approx \frac{2}{c} \ln \frac{c}{\lambda y}, \qquad \frac{\lambda y}{c} \ll 1. \qquad (84)$$

33

In general for $\lambda y^\alpha / c \ll 1$, a good approximation for $K(\lambda, y)$ is the sum of expressions in Eqs. (80, 83):

$$K(\lambda, y) \approx A\lambda^{-1+1/\alpha} + Cy^{\alpha-1}. \qquad (85)$$

Not only this approximation reproduces the correct limits in Eqs. (80) and (83), but in the limit $\alpha \to 1$ it also reduces to Eq. (84). This approximation can be obtained by splitting the k interval in the integral in Eq. (82) into two at the value $k_0 = (\lambda/c)^{1/\alpha}$ and in each resulting integral replace the denominator by the largest term in it.

Notice that for $\alpha > 1$, and in the limit of interest $\lambda y^\alpha / c \ll 1$ the first term in Eq. (85) is much greater than the second, and we can use Eq. (80) for both $K(\lambda)$ and $K(\lambda, y)$:

$$K(\lambda) \approx K(\lambda, y) \approx A\lambda^{-1+1/\alpha}, \qquad\qquad \alpha > 1. \qquad (86)$$

For $\alpha < 1$ the opposite is true, and we can use Eq. (83) as a valid approximation:

$$K(\lambda, y) \approx Cy^{\alpha-1}, \qquad\qquad C = \frac{2}{c}\Gamma(1-\alpha). \qquad (87)$$

References

[1] I. Rushkin, P. Oikonomou, L.P. Kadanoff and I.A. Gruzberg, J. Stat. Mech. P01001 (2006); arXiv: cond-mat/0509187

[2] O. Schramm, Israel J. Math. **118**, 221 (2000); arXiv: math.PR/9904022.

[3] G. F. Lawler. *Conformally invariant processes in the plane.* Mathematical Surveys and Monographs, **114**. Providence, R.I.: American Mathematical Society, 2005.

[4] W. Werner, *Random planar curves and Schramm-Loewner evolutions*, in Lecture Notes in Mathematics, **1840**. Berlin, New York: Springer-Verlag, 2004; arXiv: math.PR/0303354.

[5] O. Schramm, *Conformally invariant scaling limits: an overview and a collection of problems*, in International Congress of Mathematicians. Vol. I, 513, Eur. Math. Soc., Zürich, 2007; arXiv: math.PR/0602151.

[6] M. Bauer and D. Bernard, Phys. Rep. **432**, 115 (2006); arXiv: math-ph/0602049.

[7] J. Cardy, Ann. Phys. **318**, 81 (2005); arXiv: cond-mat/0503313.

[8] I. A. Gruzberg, J. Phys. A: Math. Gen. **39**, 12601 (2006); arXiv: math-ph/0607046.

[9] I. A. Gruzberg and L. P. Kadanoff, J. Stat. Phys. **114**, 1183 (2004); arXiv: cond-mat/0309292.

[10] W. Kager and B. Nienhuis, J. Stat. Phys. **115**, 1149 (2004); arXiv: math-ph/0312056.

[11] Q. Guan and M. Winkel, arXiv: math.PR/0606685.

[12] Q. Guan, arXiv: 0705.2321 [math.PR].

[13] Z.-Q. Chen and S. Rohde, arXiv:0708.1805v2 [math.PR].

[14] D. Beliaev and S. Smirnov, Harmonic measure and SLE, arXiv: 0801.1792v1 [math.CV].

[15] B. Duplantier, Phys. Rev. Lett. **84**, 1363 (2000); arXiv: cond-mat/9908314.

[16] B. Duplantier, in *Fractal geometry and applications: a jubilee of Benot Mandelbrot, Part 2*, 365, Proc. Sympos. Pure Math., 72, Part 2, Providence, R.I.: American Mathematical Society, 2004; arXiv: math-ph/0303034.

[17] E. Bettelheim, I. Rushkin, I. A. Gruzberg, P. Wiegmann, Phys. Rev. Lett. **95**, 170602 (2005); arXiv: hep-th/0507115.

[18] I. Rushkin, E. Bettelheim, I. A. Gruzberg, and P. Wiegmann, J. Phys. A: Math. Theor. **40**, 2165 (2007); arxiv: cond-mat/0610550.

[19] S. Rohde and O. Schramm, Ann. of Math. (2), **161**(2), 883 (2005); arXiv: math.PR/0106036.

[20] D. Appelbaum. *Lévy processes and stochastic calculus*, Cambridge, U.K.; New York: Cambridge University Press, 2004.

[21] R. Metzler and J. Klafter, Phys. Reports **339**, 1 (2000).

[22] G. Samorodnitsky and M. S. Taqqu. *Stable non-Gaussian random processes: stochastic models with infinite variance*, New York: Chapman & Hall, 1994.

[23] K. Sato. *Lévy processes and infinitely divisible distributions*, Cambridge, U.K.; New York: Cambridge University Press, 1999.

[24] M. B. Hastings, Phys. Rev. Lett. **88**, 055506 (2002); arXiv: cond-mat/9607021.